Effect of Ball-Milling on 3-V Capacity of Lithium−Manganese Oxospinel Cathodes

Sun-Ho Kang, John B. Goodenough,* and Llewellyn K. Rabenberg

Texas Materials Institute, ETC 9.102, University of Texas at Austin, Austin, Texas 78712

Received November 20, 2000. Revised Manuscript Received February 14, 2001

Ball-milling for a sufficient period of time of lithium−manganese oxide spinels, prepared either by a sol−gel method or by solid-state reaction, gave cathode materials of a lithium cell with excellent capacity retention in the 3-V range at room temperature and elevated temperatures despite an apparent Jahn−Teller distortion. In a 50-cycle test with 0.5 mA/cm^2, a sample ball-milled for 1 h gave a constant capacity of 122 mAh/g at a constant voltage 2.9 V versus lithium. X-ray diffraction and transmission electron microscopy were performed on the ball-milled spinel powders; they were found to contain significant strain and to consist of nanometer-scale grains. Furthermore, partial oxidation of manganese ions took place during the ball-milling process.

1. Introduction

The ability to insert Li reversibly into the $[Mn_2]O_4$ spinel framework makes $Li_y[Mn_2]O_4$ a potential cathode material for lithium rechargeable batteries.[1−4] Its three-dimensional Li^+-ion diffusion, low material cost, and benign environmental impact make it attractive vis à vis the $Li_{1-x}Ni_yCo_{1-y}O_2$ layered oxide presently in widespread use. Moreover, it delivers 4 V versus a lithium anode in the range $0 < y < 1$ and 3 V in the range $1 < y < 2$. However, the capacity fades sharply upon repeated charge/discharge cycling in the 3-V range, which has limited application of the lithium−manganese oxospinel (LMOS) to the 4-V range.[3, 5−8]

The capacity fading of LMOS in the 3-V range has been attributed to the Jahn−Teller distortion that occurs when the average valence of Mn falls below +3.5; lithium insertion into $Li_{1+x}[Mn_2]O_4$ electrodes ($x > 0$) is accompanied by the formation of a tetragonal phase. Although the coexistence of two phases has the beneficial effect of giving a constant output voltage versus Li of about 2.9 V over most of the discharge,[1] the increase in the axial ratio from $c/a = 1.0$ in the cubic phase to $c/a = 1.16$ in the tetragonal phase due to the cooperative Jahn−Teller distortion leads to a fracture of larger particles with a loss of electrical contact with the current collector upon repeated charge/discharge cycling.[5,9,10] Moreover, the surface disproportionation $2Mn^{3+} \rightarrow Mn^{2+} + Mn^{4+}$ is followed by dissolution of $Mn^{2+} + Li^+$ in strongly acidic (pH < 2) aqueous solution, which has led to the suggestion that dissolution of the Mn^{3+}-rich $Li_2[Mn_2]O_4$ phase may contribute to the capacity fading. Thackeray et al.[11] detected a tetragonal $Li_2[Mn_2]O_4$ phase at the surface of electrodes discharged in the 4-V range (from 4.2 to 3.3 V) and have pointed out that electrode dissolution might also contribute to capacity fading in the 4-V range.

Several strategies have been suggested to overcome the rapid capacity fading in the 3-V range: Kim and Manthiram[12] developed nanocomposite and amorphous manganese oxides to minimize the Jahn−Teller distortion problem. Following the suggestion of Thackeray to reduce the Mn^{3+} concentration in the parent compound, other papers from Manthiram's research group[14,15] have reported excellent cyclability in the 3-V range for $Li_2Mn_4O_9$ and $Li_4Mn_5O_{12}$, which initially contain only Mn^{4+} ions. Sun et al.[16−18] stabilized lithium−manganese spinels by, they presumed, doping sulfur on oxygen sites (e.g., $LiAl_{0.24}Mn_{1.76}O_{3.98}S_{0.02}$); their spinel materials exhibited improved cyclability in both the 4- and 3-V regions. Jang et al.[19,20] reported that no significant

---

* To whom correspondence should be addressed. E-mail: jgoodenough@mail.utexas.edu.

(1) Goodenough, J. B.; Thackeray, M. M.; David, W. I. F.; Bruce, P. G. *Rev. Chim. Miner.* **1984**, *21*, 435.

(2) Tarascon, J. M.; Wang, E.; Shokoohi, F. K.; McKinnon, W. R.; Colson, S. *J. Electrochem. Soc.* **1991**, *138*, 2859.

(3) Gummow, R. J.; Kock, A.; Thackeray, M. M. *Solid State Ionics* **1994**, *69*, 59.

(4) Liu, W.; Kowal, K.; Farrington, G. C. *J. Electrochem. Soc.* **1994**, *145*, 459.

(5) Thackeray, M. M.; Kock, A.; Rossouw, M. H.; Liles, D.; Bittihn, R.; Hodge, D. *J. Electrochem. Soc.* **1992**, *139*, 363.

(6) Arora, P.; Popov, B. N.; White, R. E. *J. Electrochem. Soc.* **1998**, *145*, 807.

(7) Liu, Z.; Yu, A.; Lee, J. Y. *J. Power Sources* **1998**, *74*, 228.

(8) Huang, H.; Chen, C. H.; Perego, R. C.; Kelder, E. M.; Chen, L.; Schoonman, J.; Weydanz, W. J.; Nielsen, D. W. *Solid State Ionics* **2000**, *127*, 31.

(9) Thackeray, M. M.; David, W. I. F.; Bruce, P. G.; Goodenough, J. B. *Mater. Res. Bull.* **1983**, *18*, 461.

(10) Thackeray, M. M. *Prog. Solid State Chem.* **1997**, *25*, 1.

(11) Thackeray, M. M.; Shao-Horn, Y.; Kahaian, A. J.; Kepler, K. D.; Skinner, E.; Vaughey, J. T.; Hackney, S. A. *Electrochem. Solid-State Lett.* **1998**, *1*, 7.

(12) Kim, J.; Manthiram, A. *Electrochem. Solid-State Lett.* **1998**, *1*, 207.

(13) Kim, J.; Manthiram, A. *Electrochem. Solid-State Lett.* **1999**, *2*, 55.

(14) Kim, J.; Manthiram, A. *J. Electrochem. Soc.* **1998**, *145*, L53.

(15) Choi, S.; Manthiram, A. *J. Electrochem. Soc.* **2000**, *147*, 1623.

(16) Sun, Y.-K.; Jeon, Y.-S. *J. Mater. Chem.* **1999**, *9*, 3147.

(17) Sun, Y.-K.; Jeon, Y.-S.; Lee, H. J. *Electrochem. Solid-State Lett.* **2000**, *3*, 7.

(18) Park, S. H.; Park, K. S.; Sun, Y.-K.; Nahm, K. S. *J. Electrochem. Soc.* **2000**, *147*, 2116.

(19) Jang, Y.-I.; Huang, B.; Wang, H.; Sadoway, D. R.; Chiang, Y.-M. *J. Electrochem. Soc.* **1999**, *146*, 3217.

10.1021/cm000920g CCC: $20.00

capacity fading in the 3-V range was observed in a lithium−manganese spinel obtained by conversion from the layered, orthorhombic $LiMnO_2$ during electrochemical cycling. Although the above-mentioned works have made progress in improving the cycle life of LMOS cathodes in the 3-V range, the cathode materials either lost the constant output voltage associated with the two-phase compositional range or required a complicated, multistep processing route that may introduce another toxic element.

Recently, we demonstrated that $Li[Li_yMn_{2-y}]O_4$ spinel powders, prepared by either a sol−gel or an aqueous solution method, showed excellent cyclability in the 3-V range (2.4−3.4 V) while retaining the constant output voltage associated with the apparent Jahn−Teller distortion;[21,22] the origin of the excellent cyclability was not elucidated. In an investigation to determine whether the improved cyclability was from our method of material preparation or was due to a postpreparation processing step, we found that a ball-milling process used to mix active material and carbon in our laboratory played an important role in improving the capacity retention. By X-ray diffraction (XRD) and transmission electron microscopy (TEM), it was found that the ball-milled spinel powders contained significant strain and consisted of nanograined particles. In this article, we report the effect of ball-milling on the 3-V capacity of lithium−manganese oxospinel cathodes and the nanostructural features of the ball-milled spinel particles.

2. Experimental Section

Materials Preparation and Characterization. LMOS powders were prepared by a sol−gel method and by conventional solid-state reaction; these powders are referred to as SG-LMOS and SS-LMOS, respectively. $Li(CH_3COO)\cdot 2H_2O$ (GFS Chemicals) and $Mn(CH_3COO)_2\cdot 4H_2O$ (GFS Chemicals) were used for the sol−gel method. Each of the starting materials was dissolved in distilled water and added to a 2 M aqueous solution of glycolic acid. The pH of the solution was adjusted to 8.5 with ammonium hydroxide. All of the process was conducted under continuous stirring. The solution was then heated in a beaker on a hot plate to dryness. The resulting gel precursor was decomposed at 400 °C for 10 h in air; the decomposed powders were fired at 800 °C for 6 h in air and furnace-cooled. For the solid-state synthesis, Li_2CO_3 (Fisher Scientific) and $MnCO_3$ (GFS Chemicals) were mixed and prefired at 500 °C for 10 h in air. The prefired powder was ground and then fired at 800 °C for 20 h in air and furnace-cooled with an intermittent grinding.

The as-prepared spinel powders were mixed with carbon in the weight ratio of 70:25 either by hand-grinding in an agate mortar with an ethanol medium or by ball-milling in air (Spex 8000 Mixer/Mill) with stainless-steel balls for various times. (Each spinel powder will be denoted as SG-LMOS*n* or SS-LMOS*n*, where *n* denotes ball-milling time. For example, SG-LMOS*h* indicates LMOS prepared by sol−gel and mixed with carbon by hand-grinding and SS-LMOS*15* means LMOS prepared by the solid-state reaction method and mixed with carbon by ball-milling for 15 min.) As is discussed below, the ball-milling not only provides intimate mixing to improve the electrical contact between spinel particles and carbon but also introduces lattice strain and nanostructured texture into the spinel particles.

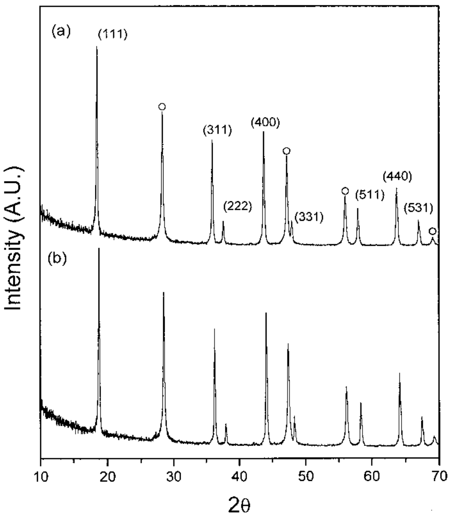

Figure 1. Powder XRD patterns of (a) SG-LMOS and (b) SS-LMOS. Open circles denote silicon internal standard.

Phase purity was verified from powder X-ray diffraction (XRD) with a Philips APD 3520 diffractometer; the lattice constant was determined from the XRD data by iterative least-squares refinements against an internal silicon standard. The morphology of the synthesized powder was observed with SEM (Hitachi S-4500) and TEM (JEOL 2010). The cationic composition was analyzed with an atomic absorption spectrophotometer (AAS, Perkin-Elmer 1100). The average oxidation state of Mn was determined by redox titration with $Na_2C_2O_4$ and $KMnO_4$.[15,21]

Electrochemical Characterization. Electrochemical characterization of the cathode materials was carried out with coin-type cells. The spinel/carbon mixtures were thoroughly mixed with poly(tetrafluoroethylene) (PTFE) by hand-grinding in a mortar. The final weight ratio of spinel:carbon:PTFE was 70:25:5. The cathode mixtures were rolled into thin sheets and cut into pellets that were typically 20−30 mg. The electrolyte was 1 M $LiClO_4$ in a 1:1 mixture of propylene carbonate (PC)/dimethoxyethane (DME) or ethylene carbonate (EC)/dimethyl carbonate (DMC). Lithium foil was used as the anode. The coin cells were fabricated in an Ar-filled glovebox. Unless specified otherwise, cells thus fabricated were cycled galvanostatically in the 3-V range of 2.4−3.3 V and the 4-V range 3.3−4.3 V at a current density of 0.5 mA/cm^2 at room temperature with an Arbin battery tester system (ABTS).

3. Results and Discussion

Materials Characterization. Powder XRD patterns of the as-prepared not ball-milled SG-LMOS and SS-LMOS are shown in Figure 1. They were identified as single spinel phases ($Fd3m$); the lattice parameters of SG-LMOS and SS-LMOS determined from the XRD patterns were 8.250(4) and 8.219(3) Å, respectively. The particle morphology of the as-prepared SG-LMOS and SS-LMOS powders are shown in Figure 2. The Li:Mn ratios of SG-LMOS and SS-LMOS determined by AAS were 1.00:2.00 and 1.05:1.95, respectively. The average oxidation states of Mn determined by the redox titration were $+3.53 \pm 0.01$ for SG-LMOS and $+3.64 \pm 0.01$ for SS-LMOS. From the Li:Mn ratio and manganese oxidation state, the overall compositions were calculated to be $Li_{0.99}Mn_{1.99}O_4$ (SG-LMOS) and $Li_{1.03}Mn_{1.91}O_4$ (SS-LMOS). The appreciable Mn deficiency in SS-LMOS indicates that $MnCO_3$ was not purely stoichiometric, probably containing surface and/or constitutional water as was pointed out by Masquelier et al.[23]

---

(20) Wang, H.; Jang, Y.-I.; Chiang, Y.-M. Electrochem. *Solid-State Lett.* **1999**, *2*, 490.

(21) Kang, S.-H.; Goodenough, J. B. *J. Electrochem. Soc.* **2000**, *147*, 3621.

(22) Kang, S.-H.; Goodenough, J. B. *Electrochem. Solid-State Lett.* **2000**, *3*, 536.

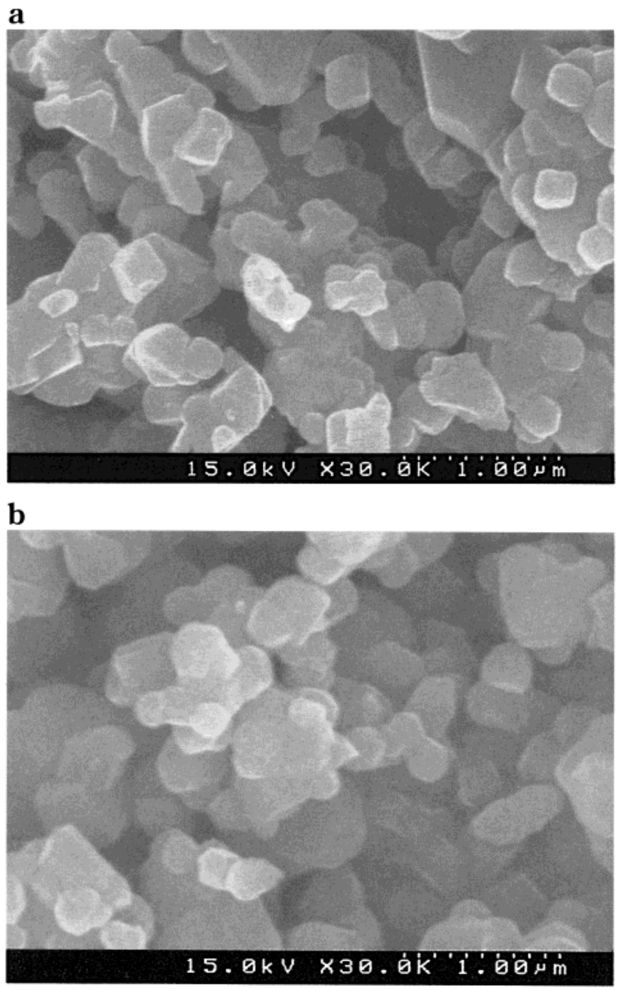

Figure 2. SEM photographs of (a) SG-LMOS and (b) SS-LMOS.

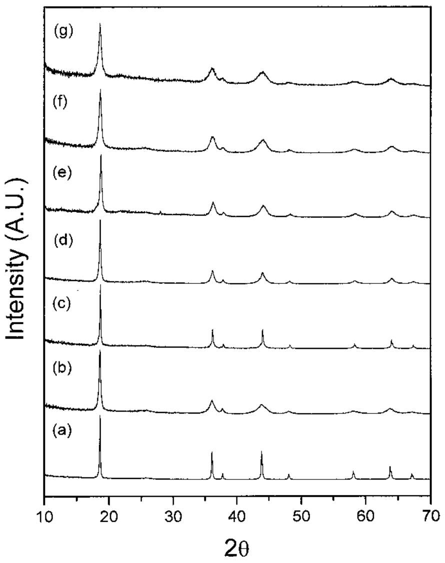

Figure 3. Powder XRD patterns of the samples: (a) SG-LMOS*h*, (b) SG-LMOS*15*, (c) SS-LMOS*5*, (d) SS-LMOS*15*, (e) SS-LMOS*30*, (f) SS-LMOS*60*, and (g) SS-LMOS*120*.

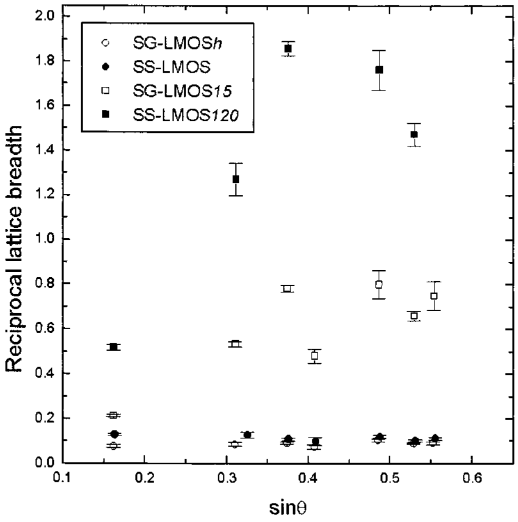

Figure 4. Reciprocal lattice breadth versus sin θ for four samples.

XRD patterns of SG-LMOS and SS-LMOS mixed with carbon either by hand-grinding or by ball-milling are shown in Figure 3. The XRD peaks of the ball-milled LMOS powders broadened remarkably; the degree of broadening increased with ball-milling time. In general, XRD peak broadening is attributed to a small crystallite size and/or lattice strain caused by structural defects such as dislocations or stacking faults.[19,24,25] Because the size broadening is independent of the reciprocal space variable d^* ($d^* = 2 \sin \theta/\lambda$) and the strain broadening scales with d^*, the origin of the peak broadening can be determined from the dependence of β^* on sin θ, where β^* denotes reciprocal lattice breadth.[24] The reciprocal lattice breadth of each powder was calculated by fitting each XRD pattern to a pseudo-Voigt function with the JADE program[26] and typical results are shown in Figure 4. The reciprocal lattice breadths of un-milled powders (SG-LMOS, SS-LMOS, and SG-LMOS*h*) were almost independent of sin θ, which indicates that strain was negligible in those powders. On the other hand, the reciprocal lattice breadths of the ball-milled spinel powders were found to be strongly dependent on sin θ, which is typical of strain broadening. However, a precise deconvolution of the crystallite size and strain broadening in the ball-milled spinel particles could not be made from the total peak broadening due to a lack of data points and large scattering.

TEM images and selected-area diffraction (SAD) patterns of the as-prepared SS-LMOS, SS-LMOS*60*, and SS-LMOS*120*, where the final number indicates the time in minutes in the ball-mill, are shown in Figure 5. The as-prepared SS-LMOS particle consisted of clean spinel crystals; the SAD was a spotty ring. However, SS-LMOS*60* and SS-LMOS*120* particles displayed nanometer-scale grains with (111) fringes in random orientation and SAD patterns of faint rings. It was observed that some SS-LMOS*60* and SS-LMOS*120* particles contained larger (20−40 nm) grains that revealed diffraction contrast images of intense bend contours. These nanocrystalline grains and strain developed at grain boundaries would give rise to the XRD peak broadening in Figure 3. Although the mechanism

---

(23) Masquelier, C.; Tabuchi, M.; Ado, K.; Kanno, R.; Kobayashi, Y.; Maki, Y.; Nakamura, O.; Goodenough, J. B. *J. Solid State Chem.* **1996**, *123*, 255.

(24) Williamson, G. K.; Hall, W. H. *Acta Metal.* **1953**, *1*, 23.

(25) Klug, H. P.; Alexander, L. E. In *X-ray Diffraction Procedures: For Polycrystalline and Amorphous Materials*; John Wiley & Sons: New York, 1974; p 661.

(26) JADE, Release 5.0.25, Materials Data, Inc., Livermore, 2000.

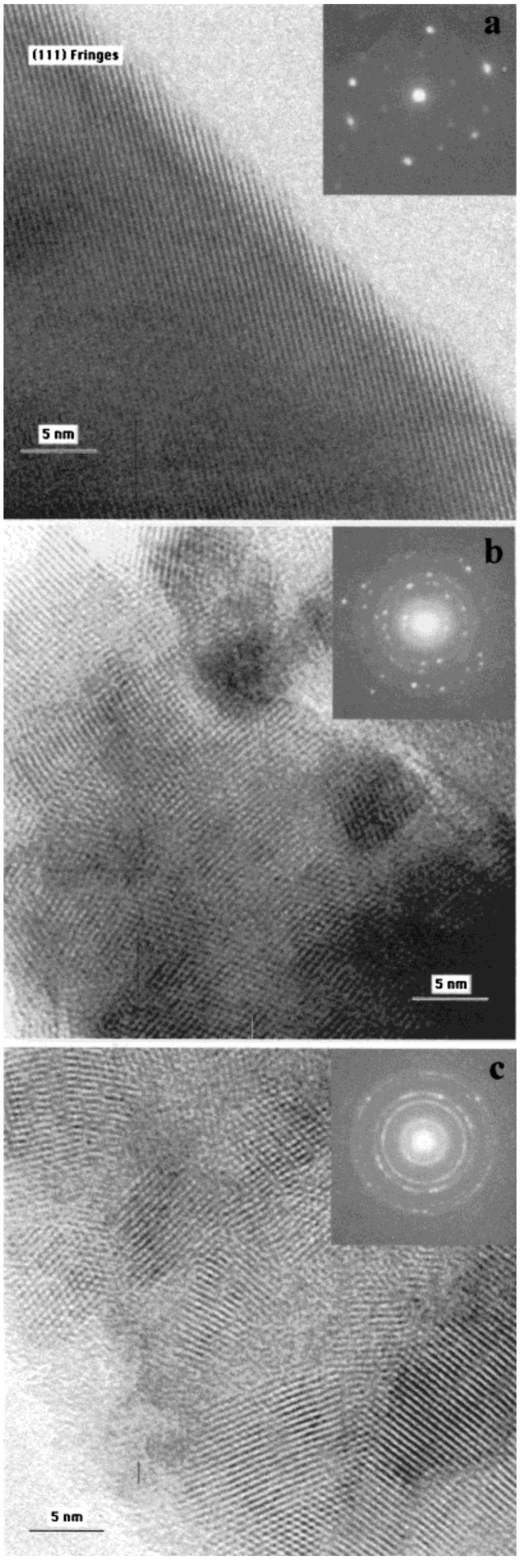

Figure 5. TEM photographs and selected area diffraction patterns of the samples: (a) as-prepared SS-LMOS, (b) SS-LMOS*60*, and (c) SS-LMOS*120*. Each of the diffraction patterns is consistent with the spinel structure. For the nanocrystalline grains in SS-LMOS*60* and SS-LMOS*120*, rings for {111}, {222} and {311}, {400}, {333} and {511}, {440} and {531} are observed. JCPDS Card no. 35-0782 lists these as the strong lines for X-ray diffraction from $LiMn_2O_4$. The single-crystal pattern from SS-LMOS is near the [011] orientation; weak {111} and (by double diffraction) {200} reflections appear near the origin; stronger $\{31\bar{1}\}$ and $\{22\bar{2}\}$ form what appear to be an "ellipse."

of formation of the nanosize grains through the ball-milling is not established at this stage, we suggest two possibilities: (1) the particles were broken into nanoparticles that subsequently were stuck back together to become hard agglomerates during the ball-milling process; (2) many nanograins were generated within a big crystallite by the action of defects, for example, dislocations, during the ball-milling.

Chemical titration was carried out with the ball-milled spinel powders. (For redox titration, SG-LMOS and SS-LMOS were ball-milled without carbon.) The average manganese oxidation state of SG-LMOS was found to increase from +3.53 ± 0.01 to +3.65 ± 0.01 after ball-milling for 15 min, which means that the overall composition of SG-LMOS*15* changed to $Li_{0.96}Mn_{1.93}O_4$ because ball-milling is not expected to change the Li:Mn ratio. Elemental analysis was also performed on the ball-milled powders with an EDS attachment to the TEM; no Fe from the steel balls was detected. There was no change in the manganese oxidation state of SS-LMOS*5*, but it increased to +3.76 ± 0.01 in SS-LMOS powders ball-milled for longer than 15 min, which corresponds to the change of overall composition to $Li_{1.00}Mn_{1.86}O_4$. Ball-milling is known to change the oxidation state of a transition-metal oxide. Zhou et al.[27] have reported that a small amount of rhombohedral $LaCuO_3$, which is almost impossible to obtain under normal processing conditions, was observed after ball-milling $La_{1-x}Nd_xCu_2O_4$, which means that Cu was oxidized from 2+ to 3+ by the ball-milling. On the other hand, Linderoth et al.[28] reported that α-Fe_2O_3 was reduced to Fe_3O_4 by high-energy ball-milling.

In conclusion, the ball-milling process altered the particle characteristics significantly in three respects: (1) formation of nanometer-scale grains in a particle, (2) generation of lattice strain, and (3) partial oxidation of manganese ions.

Electrochemical Properties. The charge/discharge curves of Li/SG-LMOS*n* (*n* = *h*, *15*, where *h* stands for hand-ground) cells in the 3-V range of 2.4−3.4 V at a current density of 0.5 mA/cm^2 are shown in Figure 6; the corresponding discharge capacity as a function of cycle number is given in Figure 7. Note that the cycling behavior of SG-LMOS*h* is much different from that of SG-LMOS*15*. SG-LMOS*h* delivered an initial capacity of 136 mAh/g, but the capacity decreased sharply with successive cycles. In contrast, the initial capacity of SG-LMOS*15* was only 104 mAh/g. However, after it showed an initial drop to 98 mAh/g at the second cycle, the capacity of SG-LMOS*15* increased slowly with further cycling and was stabilized at ca. 122 mAh/g after the 15th cycle. At the same time, the overvoltage decreased and the flatness of the plateaus was improved with cycling; a flat plateau is indicative of the two-phase region of cubic and tetragonal phases.[1] This behavior was reproducible. The charge/discharge curves of Li/SG-LMOS*n* (*n* = *h*, *15*) cells in the 4-V range (3.3−4.3 V) at a current density of 0.5 mA/cm^2 are shown in Figure 8; the corresponding discharge capacity as a function of cycle number is given in Figure 9. The initial

---

(27) Zhou, J.-S.; Archibald, W.; Goodenough, J. B. *Phys. Rev. B* **2000**, *61*, 3196.

(28) Linderoth, S.; Jiang, J. Z.; Morup, S. *Mater. Sci. Forum* **1997**, *235−238*, 205.

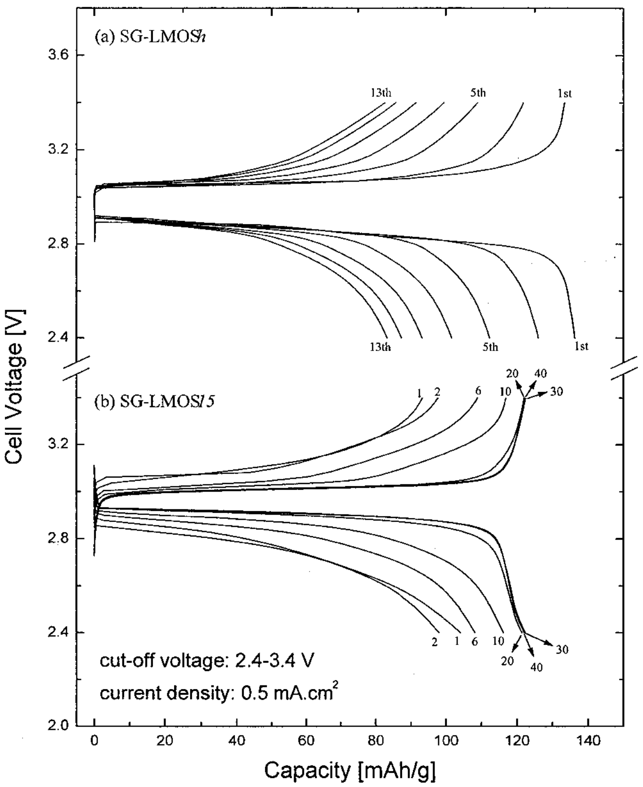

Figure 6. Charge/discharge curves of (a) SG-LMOS*h* and (b) SG-LMOS*15* in the voltage range of 2.4−3.4 V at a current density of 0.5 mA/cm^2.

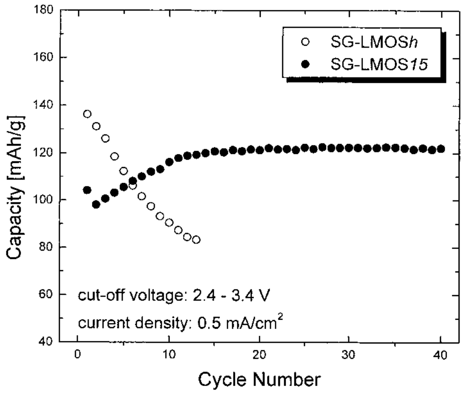

Figure 7. Discharge capacities of Li/SG-LMOS*h* and Li/SG-LMOS*15* cells as a function of cycle number in the voltage range of 2.4−3.4 V at a current density of 0.5 mA/cm^2.

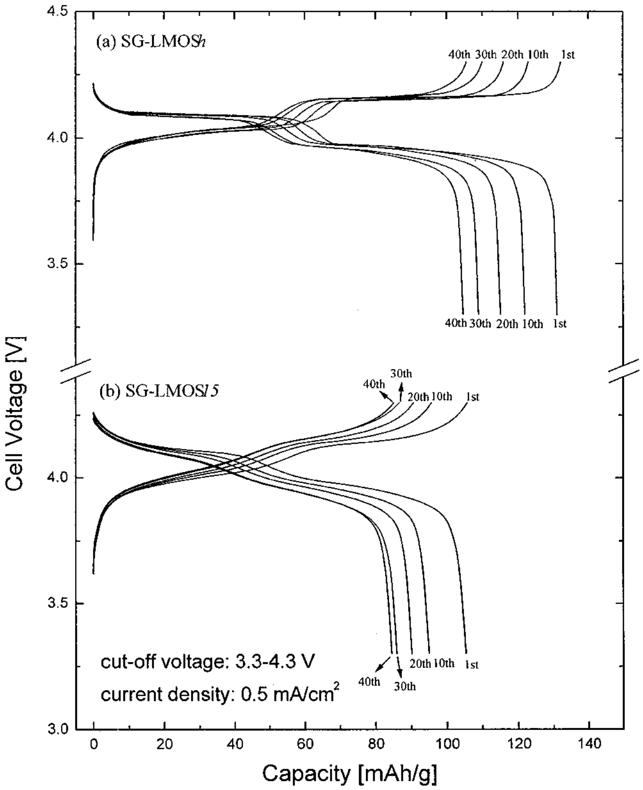

Figure 8. Charge/discharge curves of (a) SG-LMOS*h* and (b) SG-LMOS*15* in the voltage range of 3.3−4.3 V at a current density of 0.5 mA/cm^2.

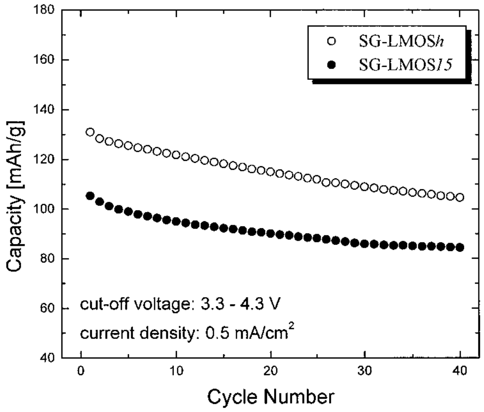

Figure 9. Discharge capacities of Li/SG-LMOS*h* and Li/SG-LMOS*15* cells as a function of cycle number in the voltage range of 3.3−4.3 V at a current density of 0.5 mA/cm^2.

discharge capacity of SG-LMOS*h* is larger, but it faded at a little higher rate than that of SG-LMOS*15*. The smaller capacity of SG-LMOS*15* is attributed to a smaller 4-V theoretical capacity because the composition was changed to $Li_{0.96}Mn_{1.93}O_4$ from $Li_{0.99}Mn_{1.99}O_4$ by the ball-milling. Another striking difference between the two materials is that SG-LMOS*h* exhibited clear plateaus near 4.17 V (upon charging) and 4.08 V (upon discharging) while the plateaus were much less pronounced for SG-LMOS*15*. The plateau at ca. 4.1 V for $Li_y[Mn_2]O_4$ is known to be due to a two-phase compositional range: one phase has $y \approx 0.2$ in which lithium ions are distributed randomly on octahedral sites and the other is $Li_{0.5}Mn_2O_4$ with lithium ions on half the tetrahedral sites in an ordered manner.[1,29] Disappearance of the flat plateau at ca. 4.1 V is found for lithium-excess manganese spinels, that is, $Li[Li_yMn_{2-y}]O_4$.[3,30] Oxidation of the Mn by ball-milling is charge-compensated in a spinel by the introduction of cation vacancies. As cation vacancies were generated by the ball-milling, it is presumed that some Li ions were displaced to the vacant 16d octahedral sites due to an octahedral-site preference of Li.[31] The experimental results in Figures 6−9 show clearly how the electrochemical properties of a lithium−manganese oxide spinel are influenced by ball-milling.

Figures 10 and 11 present the charge/discharge curves and discharge capacity, respectively, of Li/SS-

---

(29) Ohzuku, T.; Kitagawa, M.; Hirai, T. *J. Electrochem. Soc.* **1990**, *137*, 769.

(30) Nishimura, K.; Douzono, T.; Kasai, M.; Andou, H.; Muranaka, Y.; Kozono, Y. *J. Power Sources* **1999**, *81−82*, 420.

(31) Rogers, B. D.; Germann, R. W.; Arnott, R. J. *J. Appl. Phys.* **1965**, *36*, 2338.

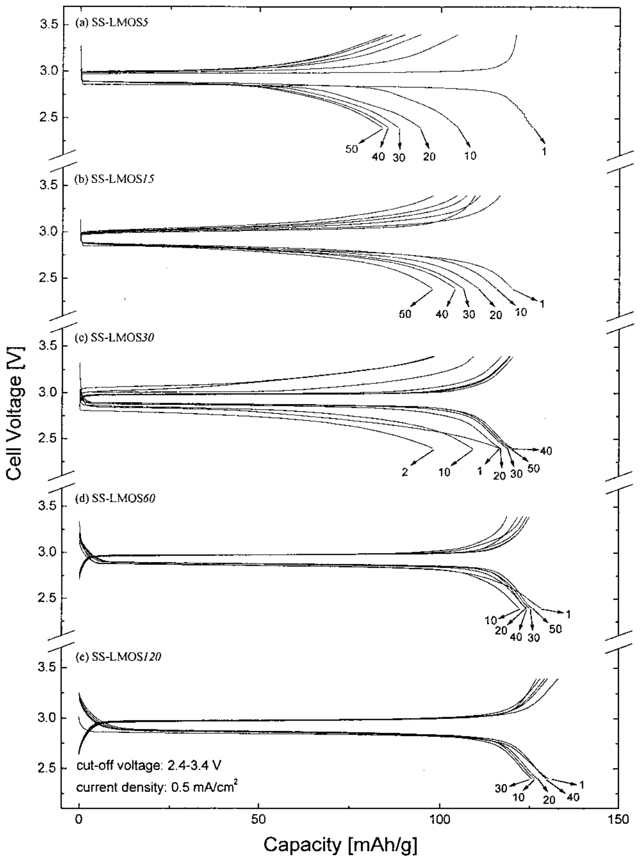

Figure 10. Charge/discharge curves of SS-LMOS*n* ($n = 5$, 15, 30, 60, and 120 min) in the voltage range of 2.4−3.4 V at a current density of 0.5 mA/cm^2.

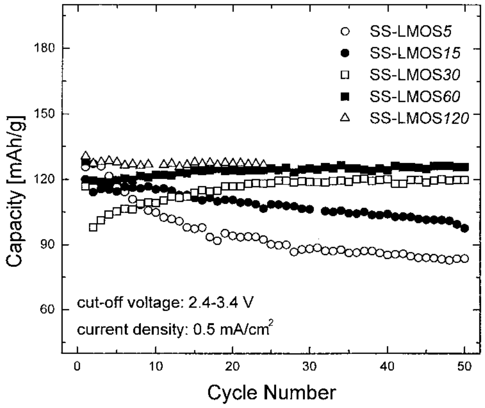

Figure 11. Discharge capacities of Li/SS-LMOS*n* ($n = 5$, 15, 30, 60, and 120 min) cells as a function of cycle number in the voltage range of 2.4−3.4 V at a current density of 0.5 mA/cm^2.

LMOS*n* ($n = 5$, 15, 30, 60, and 120 min) cells in the 3-V range at a current density of 0.5 mA/cm^2. These results show the effect of ball-milling time on the charge/discharge curves and capacity of LMOS cathodes. SS-LMOS*5* and SS-LMOS*15* showed a continuous capacity decrease with cycling. SS-LMOS*30* exhibited similar cycling behavior to SG-LMOS*15*: a slow increase to stable capacity of 120 mAh/g after an initial drop and improvement of the flatness of plateaus with cycling. SS-LMOS*60* and SS-LMOS*120* showed much better cycling performance and revealed flat plateaus from the first discharge. SS-LMOS*60* was tested at elevated temperatures: the discharge curves and capacity are given in Figures 12 and 13, respectively. SS-LMOS*60* showed good cyclability also at 60 °C; a small capacity fading at a rate of ca. 0.1%/cycle was observed at 80 °C.

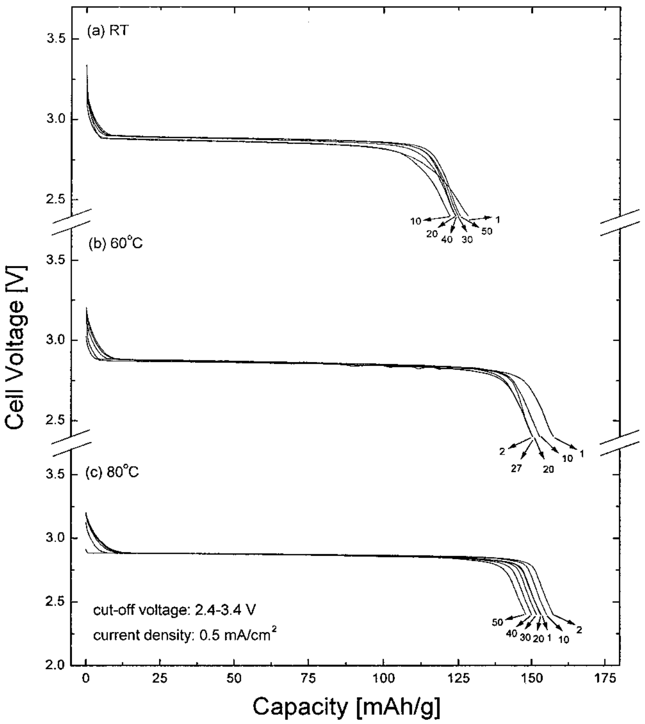

Figure 12. Discharge curves of SS-LMOS*60* in the voltage range of 2.4−3.4 V at various temperatures.

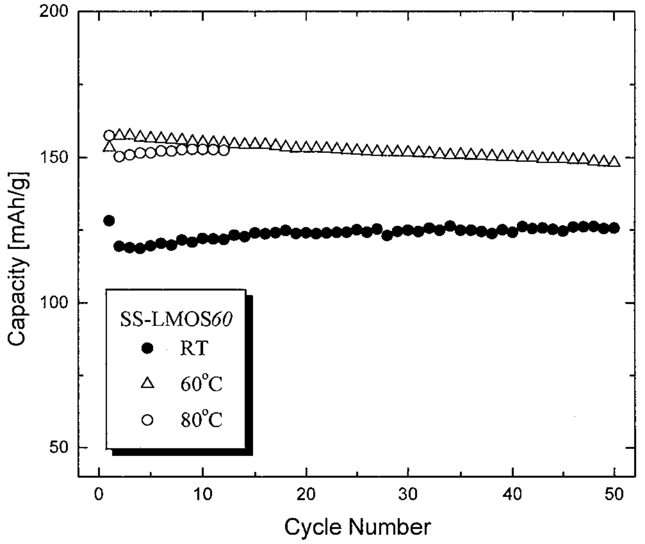

Figure 13. Discharge capacities of Li/SS-LMOS*60* cells as a function of cycle number in the voltage range of 2.4−3.4 V at various temperatures.

The improved cyclability in the presence of the Jahn−Teller orbital ordering is attributed to nanograins and strain within the cathode particles. If a spinel particle consists of very small grains, the deformation of each grain due to the formation of the tetragonal phase occurs in random directions; consequently, the net deformation of a particle with smaller grains is less anisotropic than a particle with larger grains and there is less possibility of fracture of particles due to the tetragonal distortion. Furthermore, the strain imposed by the formation of the tetragonal phase is expected to be accommodated by the already existing strain in the particle. Jang et al.[19] reported that no significant capacity fading in the 3-V range was observed in a lithium–manganese spinel obtained by conversion from the layered, orthorhombic $LiMnO_2$ during electrochemical cycling. They attributed the excellent cyclability of their spinel cathode to a nanodomain structure and strain present in the spinel particles that were introduced during the electrochemical cycling.[19,20] Although the origin of the nanometer-scale domains (grains in this work) and strain were different, we suspect that they might play the same role in improving the capacity retention of the LMOS cathodes in the 3-V range. Comparison of the electrochemical properties among SS-LMOS cathodes that were ball-milled for different times suggests there is a critical grain size and/or strain necessary for the material to exhibit excellent cyclability in the 3-V range despite the apparent Jahn–Teller distortion. Furthermore, a different ball-milling time is required for differently prepared LMOS's to have improved cyclability. (See the difference between SG-LMOS*15* and SS-LMOS*15*.) An SS-LMOS*60* cathode was examined by XRD and TEM after cycling; almost no changes in the XRD patterns and nanograin features were found in the cycled cathode material.

4. Conclusions

Lithium–manganese oxospinel powders were prepared by a sol–gel method (SG-LMOS) and by a solid-state reaction method (SS-LMOS); these powders were ball-milled for various periods of time. A SG-LMOS powder ball-milled for 15 min showed no capacity fading in the 3-V range during extended electrochemical cycling despite the apparent Jahn–Teller distortion, while un-milled SG-LMOS powder showed the rapid capacity fading generally found for LMOS cathodes. SS-LMOS powders were ball-milled for various periods of time (5, 15, 30, 60, and 120 min); the cycling performance in the 3-V range improved with ball-milling time; ball-milling for longer than 30 min was necessary to achieve acceptable cyclability. An SS-LMOS cathode ball-milled for 60 min showed excellent cyclability also at elevated temperatures (60 and 80 °C). XRD, TEM, and redox titration revealed that the ball-milled spinel particles contained significant strain, consisted of nanograins, and had a higher manganese oxidation state than un-milled spinel particles. It was concluded that all these features contributed to the improved cycling performance in the 3-V range. The results in this work suggest a simple and effective way to stabilize the 3-V cyclability of lithium–manganese oxospinel cathodes for rechargeable lithium batteries.

Acknowledgment. We thank the Hydro-Quebec Corporation and the Robert A. Welch Foundation, Houston, TX, for financial support.

CM000920G